Earthq Eng & Eng Vib (2010) 9: 555-567 **DOI**: 10.1007/s11803-010-0037-x

Seismic response of underground utility tunnels: shaking table testing and FEM analysis

Jiang Luzhen[2†], Chen Jun[1,2‡] and Li Jie[1,2§]

1. *State Key Laboratory for Disaster Reduction in Civil Engineering, Tongji University, Shanghai 200092, China*

2. *Department of Building Engineering, Tongji University, Shanghai 200092, China*

Abstract: Underground utility tunnels are widely used in urban areas throughout the world for lifeline networks due to their easy maintenance and environmental protection capabilities. However, knowledge about their seismic performance is still quite limited and seismic design procedures are not included in current design codes. This paper describes a series of shaking table tests the authors performed on a scaled utility tunnel model to explore its performance under earthquake excitation. Details of the experimental setup are first presented focusing on aspects such as the design of the soil container, scaled structural model, sensor array arrangement and test procedure. The main observations from the test program, including structural response, soil response, soil-structure interaction and earth pressure, are summarized and discussed. Further, a finite element model (FEM) of the test utility tunnel is established where the nonlinear soil properties are modeled by the Drucker-Prager constitutive model; the master-slave surface mechanism is employed to simulate the soil-structure dynamic interaction; and the confining effect of the laminar shear box to soil is considered by proper boundary modeling. The results from the numerical model are compared with experiment measurements in terms of displacement, acceleration and amplification factor of the structural model and the soil. The comparison shows that the numerical results match the experimental measurements quite well. The validated numerical model can be adopted for further analysis.

Keywords: lifeline system; utility tunnel; shaking table test; finite element method; soil-structure interaction

1 Introduction

Fast population growth and concentrations in urban areas, as a global phenomenon, has resulted in a significant shortage of aboveground space, and has therefore led to increased development of underground structures. As far as the modern city lifeline system is concerned, the most attractive way, at least in China, for construction is the adoption of an underground utility tunnel. A utility tunnel, once called a pipe subway, is a type of underground structure that accommodates various utilities such as water, sewage, gas, electrical power, telephone and heat supply, and also provides enough head-room to allow maintenance personnel access to perform maintenance tasks. The use of a multi-purpose utility tunnel to integrate urban services is a key for issues related to the construction of lifeline systems, such as congestion in shallow underground areas, traffic interruption, environmental preservation, among many others. Therefore, utility tunnels have been widely constructed throughout the world since their first use in Paris in 1833.

Being the carrier for many utility pipes, the performance of utility tunnels under earthquake is of great importance for the safety of these urban lifeline systems. The utility tunnels are linear and cut-and-cover structures whose cross sections are typically smaller than traffic tunnels and larger than underground pipelines. Experience from major earthquakes has shown that cut-and-cover tunnels are more vulnerable to an earthquake event than circular bored tunnels (Hashash *et al*., 2001). For instance, in the 1995 Hyogoken-Nambu earthquake, different types of damage were observed to almost all utility tunnels near the epicenter (JSCE, 1999; PWRI, 2001; Schiff, 1998). In the No. 2 Kobe utility tunnel, which has a double span and double-layer cross-section, cracks were found on all the corners of the tunnel cross-section, and cut-through cracks were found on the middle columns along the longitudinal axis of the tunnel at its lower layer. Many tunnel joints dislocated due to soil liquefaction or movement of surrounding soil. The inner concrete layer spalled and a water-tight slab was damaged. On the exterior surface of the tunnel, cracks along the longitudinal axis were significant in the area

Correspondence to: Chen Jun, Department of Building Engineering, Tongji University, 1239 Siping Road, Shanghai 200092, China
Fax: +86-21-65986345
E-mail: cejchen@tongji.edu.cn
†PhD Candidate; ‡Associate Professor; §Distinguished Professor

Supported by: Key Project in the National Science & Technology Pillar Program Under Grant No. 2006BAJ03B03 and Research Fund for Young Teacher Supported by State Key Laboratory for Disaster Reduction in Civil Engineering Under Grant No. SLDRCE08-C-03
Received December 31, 2009; **Accepted** September 2, 2010

where a soil mixing wall (SMW) remained and circular cracks around the cross-section were significant where the SMW did not hold together. In current practice, public utility tunnels are often constructed using an open-excavation method, and their seismic performance is similar to traditional underground tunnels for transportation despite that they have small cross-sections and are generally very shallow. It is important to assess the seismic performance of utility tunnels and to allow them to remain functional during and after a disaster. This problem is of particular importance in China because it has not been covered by current design codes, but more and more utility tunnels are being designed and built in earthquake prone areas.

Much effort has been made to determine the seismic performance of utility tunnels. PWRI (2001) summarized and reviewed damage to utility tunnels in the 1995 Hyogoken-Nambu earthquake. Nishioka and Unjo (2002) proposed a simplified evaluation method for the seismic performance of underground utility tunnels with rectangular cross sections. Nakanura *et al.* (2006) studied a side wall of utility tunnel experimentally, and found that the as-built tunnel failed in shear at the wall-slab joint. Retrofit using bolts and CFRP is effective to enhance the shear capacity and ductility. Yue and Li (2009) investigated the seismic response of a utility tunnel through numerical simulation. They revealed that the utility tunnel exhibited a global bending deformation pattern under shear wave excitation. However, the above research on the seismic response of utility tunnels is limited to theoretical analysis or numerical simulations. No experimental study of the seismic performance of utility tunnels on a shaking table has been reported. To this end, a series of shaking table test were conducted by the authors of this paper (Chen *et al*., 2010) on a scaled utility tunnel model. In this paper, a detailed description of the experimental setup is provided, focusing on the design of the soil container, soil tested and the scaled structural model, instrumentation and test procedure. The main results obtained from the test are summarized and discussed. Further, a finite element model (FEM) of the test utility tunnel is established in which the nonlinear soil property is modeled by the Drucker-Prager constitutive model; the master-slave surface mechanism is employed to simulate the soil-structure dynamic interaction; and the confining effect of the laminar shear box to soil is considered by proper boundary modeling. The results obtained from the suggested numerical model are compared with experiment measurements in terms of displacement, acceleration and amplification factor of the structural model and soil. The comparisons show that the numerical results match the experimental measurements quite well. The applicability of the suggested numerical model is validated and can be adopted for further analysis.

2 Shaking table test

2.1 Soil container

The soil container used in the test is a laminar shear box with overall dimensions of 3.00 m long (x), 1.80 m wide (y) and 1.91 m high (z). It comprises 16 steel frames stacked on each other, numbered as No.1 to No.16 from bottom to top (Fig. 1). Each frame is made of a square steel tube of 100 mm × 100 mm × 2 mm (width×height×thickness). For the adjacent frame, steel plates with a V-shaped guide (denoted as guide hereafter) were welded on the bottom of the upper frame and on the top of the lower frame. There are a total of six (four) pairs of guides mounted along the x (y) direction, three (two) for each side. High strength stainless steel balls of 1.15 cm in diameter were placed in the guide; therefore, each frame can move freely in either the x or y direction. The outer surfaces of the box were coated

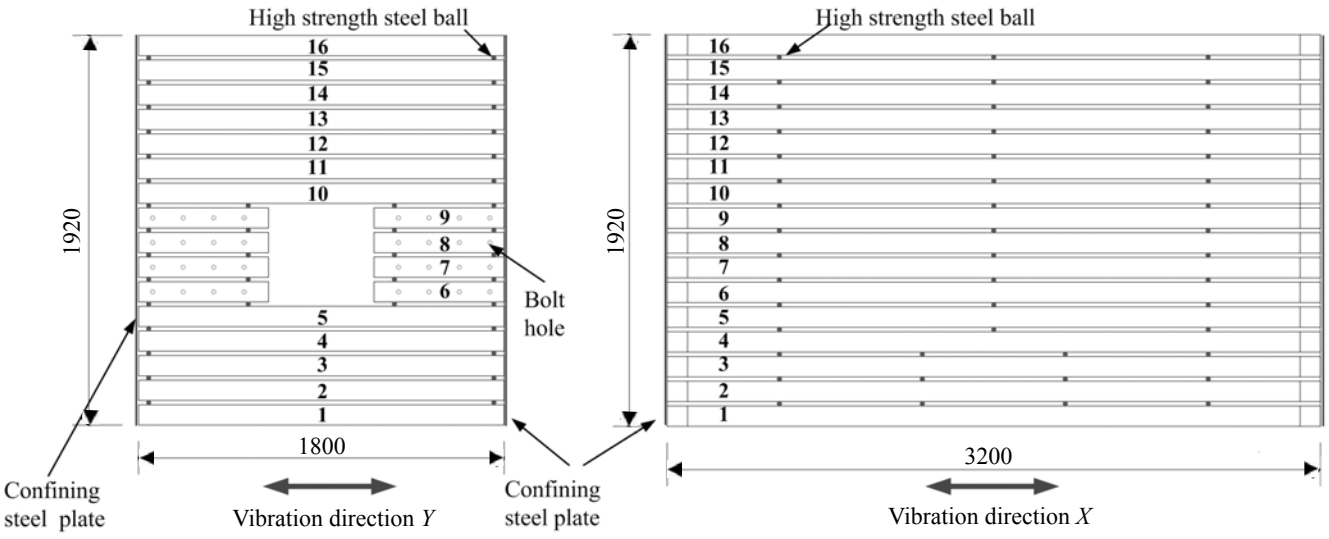

Fig. 1 The Lamina shear box (length unit: mm)

by four steel plates (named as confining plates) of 1 mm thickness. The confining plates were fixed on the frames by a number of small bolts. During the shaking table test, two confining plates on the surfaces along the vibration direction were removed. The total weight of the empty box is 2792 kg. The bottom of the box was a steel plate of 5 mm thickness welded to the frame. Finally, the shear box was bolted firmly on the shaking table using a total of 20 bolts of high tensile strength.

2.2 Tunnel model and model ground

The prototype structure for the test model is a newly-built utility tunnel in Shanghai. It has a square cross section of 3000 mm × 3000 mm and the thickness of all the walls is identical at 300 mm. Considering the capacity of the testing facility, the structure model was built with a geometrical scale of 1:5 as shown in Fig. 2. The similarity laws of the test are summarized in Table 1.

Unsaturated clay soil was used in the test. During the test, soil was placed into a shear box in layers of about 20 cm thickness. Each layer was tamped to achieve a certain density. After the soil was placed in the box, its properties were tested on a dynamic triaxial test system using samples taken directly from the shear box. Table 2 summarizes the test results of the soil properties. In this paper, model ground and tested soil has the same meaning.

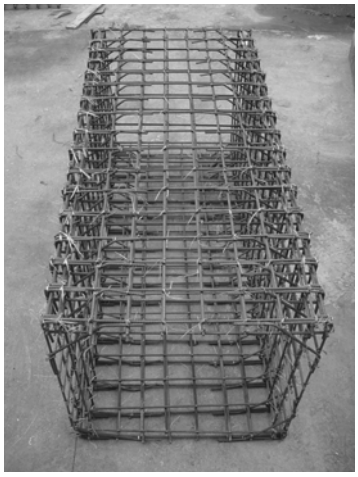

(a) Model reinforcement box

(b) Model structure

Fig. 2 Model structure

Table 1 Similarity relationships and ratios of model system

Item	Physical parameters	Similarity relation	Ratio of similarity
Geometry relation	Length	λ_L	1/5
	Displacement	λ_l	1/5
Material relation	Strain	λ_ε	1
	Stress	$\lambda_\sigma = \lambda_E \lambda_\varepsilon$	1
	Elastic module	λ_E	1
	Density	$\lambda_\rho = \lambda_E / (\lambda_a \lambda_L)$	5/3
	Mass	$\lambda_m = \lambda_E \lambda_L^2 / \lambda_a$	1/75
Dynamic relation	Frequency	$\lambda_f = \sqrt{\lambda_a / \lambda_L}$	$\sqrt{15}$
	Acceleration	λ_a	3
	Time	$\lambda_t = \sqrt{\lambda_L / \lambda_a}$	$\sqrt{1/15}$

Table 2 Physical properties of soil

Soil particle special density, d_S	Dry density, ρ_d (g/cm^3)	Void ratio, e	Cohesive strength (KPa)	Internal friction angle (º)
2.72	1.53	0.943	24.4	27.9

2.3 Instrumentation

Accelerometers, earth pressure cells, wired displacement transducer, laser displacement sensor and strain gauges were installed on the structure, in the soil, and on the soil container in order to measure the response of structure, soil and the shear box. In particular, a special device was designed to measure slippage at the interface of the structure model and the soil (Shi *et al*., 2008). The arrangement of all these sensors is depicted in Fig. 3, where the sensor names start with A, D, S, CS, EP and MD are, respectively, accelerometer, displacement transducer, soil pressure cell in the soil, concrete strain gauge, earth pressure cell attached to the structure model and displacement transducer inside the model.

2.4 Test cases

The El-Centro earthquake wave was used as the input excitation. To avoid the adverse effect of damage accumulation on the test results, only three test cases were considered. The peak ground accelerations (PGAs) in these three cases are 0.1 g, 0.4 g and 1.0 g, respectively. In addition, an additional case under sine wave excitation of acceleration amplitude of 1.0 g was also included in the model test. The frequency of the sine wave is taken as the fundamental frequency of the soil-structure system. Figure 4 shows the time history and spectrum of the input excitation. More information about the shaking table tests can be found in Shi *et al*. (2008).

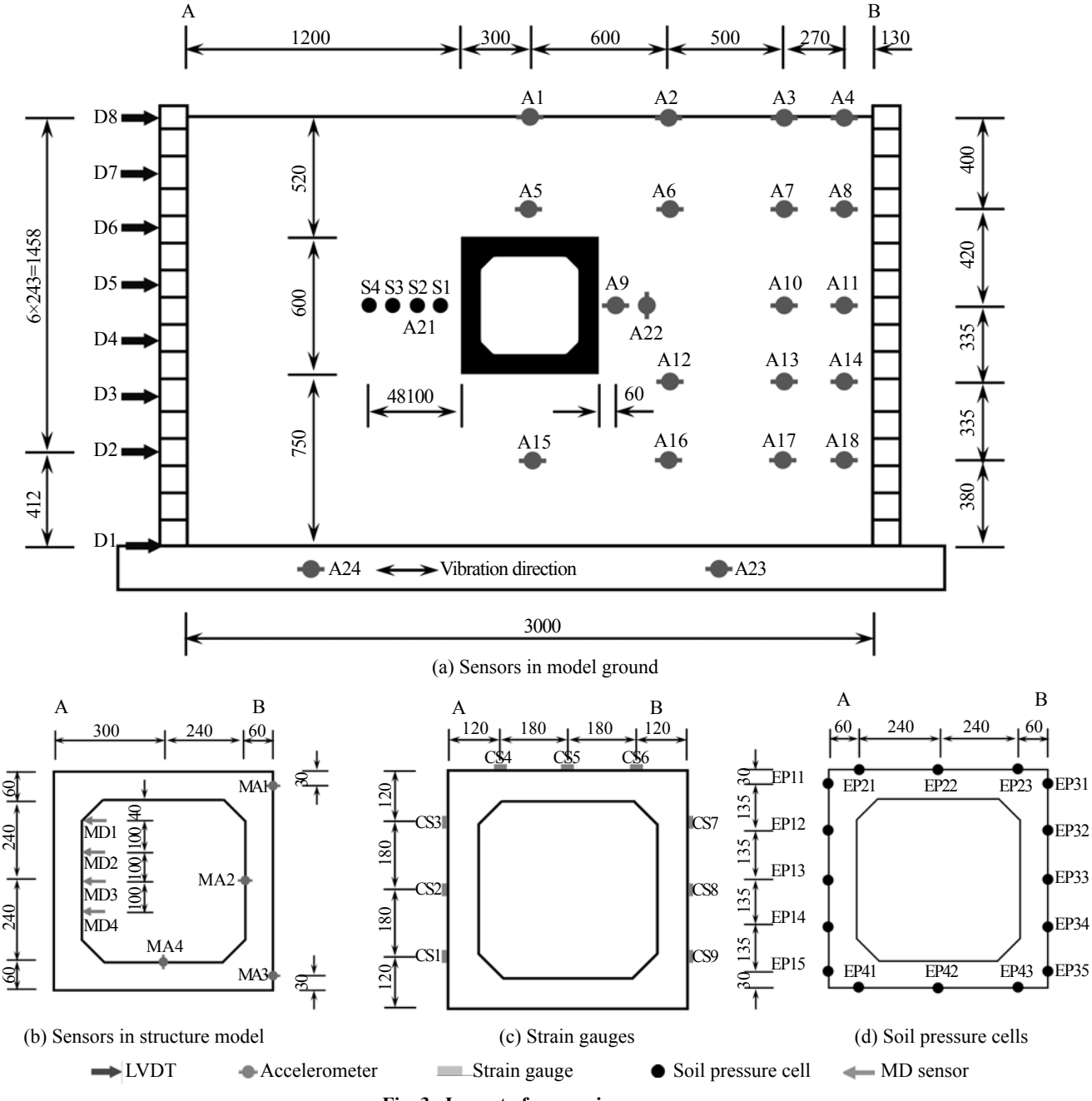

(a) Sensors in model ground

(b) Sensors in structure model

(c) Strain gauges

(d) Soil pressure cells

Fig. 3 Layout of measuring sensors

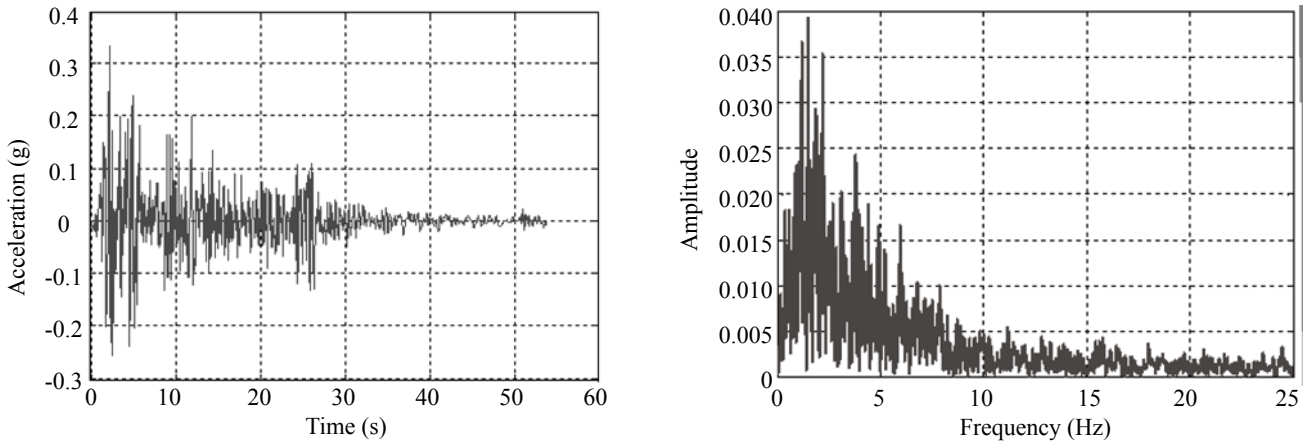

Fig. 4 Acceleration time history and Fourier spectrum of El Cento wave

3 Test results and discussion

3.1 Acceleration response

In order to find the difference of responses between the structural model and the surrounding soil, the acceleration response and its spectrum from sensors MA1, MA3 (installed on the structural model) and A6, A12 (in the soil, see Fig. 3(c)) for test case of PGA =1.0 g are compared in Fig. 5. Note that no significant time-delay between the structural response and the soil response is observed, and the amplitude of the structural response is slightly smaller than the soil response, which is consistent with observations in field measurement during earthquakes. As for the spectrum, it is seen that the spectrum of structural response and soil response are almost the same.

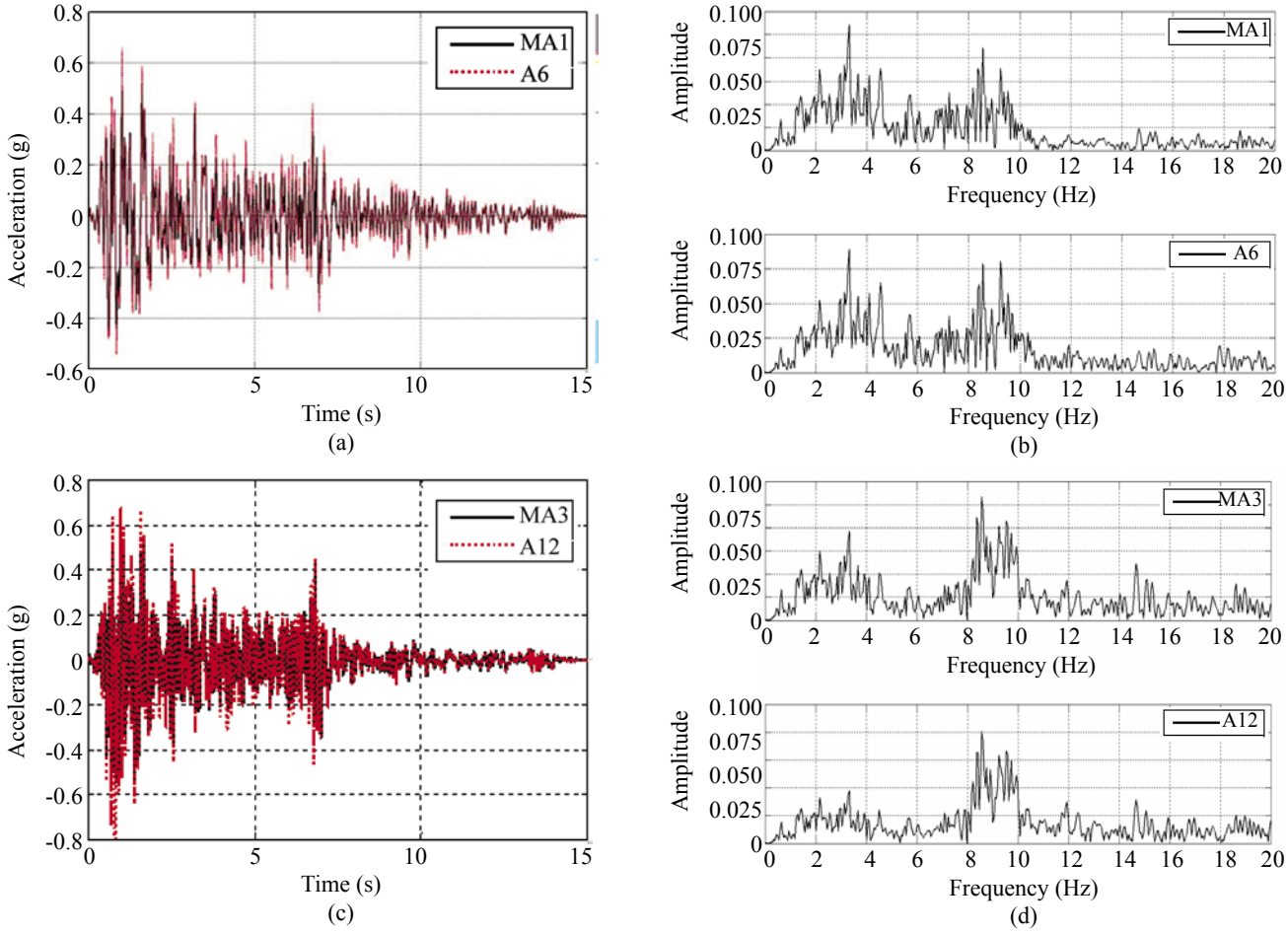

Fig. 5 Acceleration time histories and Fourier spectra of model structure and ground

3.2 Steel strains

The distributions of steel strains along different sides measured by different sensors at the time instant when the layer drift of the laminar box reaches the maximum value are shown in Fig. 6 for PGA=0.4 g, 1.0 g and sine wave with PGA=1.0 g. Note that the maximum strain occurs near the top and bottom corner of the side wall, the strain at the middle height of the side wall is almost zero, while the inner and outer steel bars are in different states (tension/compress). If the maximum steel strains from all the sensors are considered (see Shi *et al*., 2008), the distribution is slightly different from that shown in Fig. 6. Nevertheless, all the results demonstrate a clear shear deformation of the tunnel section as shown in Fig. 7, a major deformation pattern for tunnels with relatively large cross-sections.

3.3 Soil-structure interaction

Figure 8 shows the distribution of soil pressures at the time instant when the maximum story drift of the

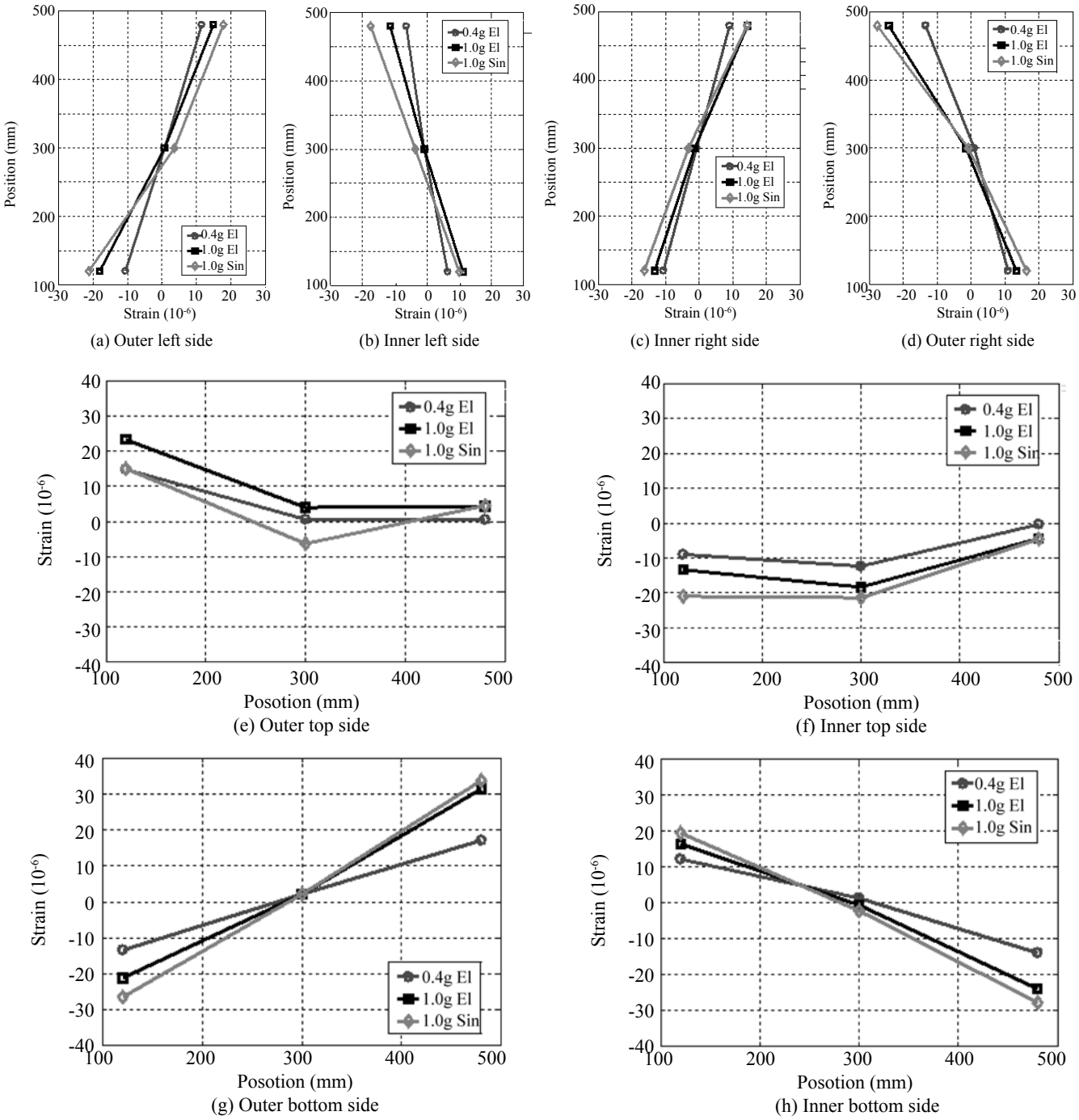

Fig. 6 Strain amplitude of the steel bar in structure

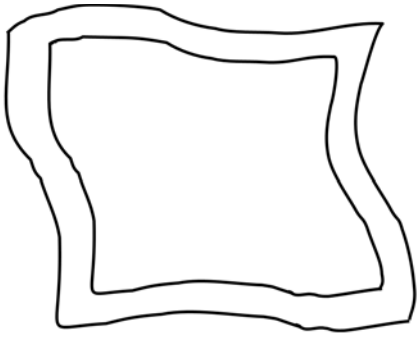

Fig. 7 Sketch of structure distortion

laminar box is reached. Note that the earth pressure is symmetrically distributed on the left and right side walls as expected, which means that when the earth pressure is negative on the left side wall, it is positive on the right side wall. The earth pressure takes a triangle distribution on the top and bottom slab. It is inferred from the above phenomena that the shear deformation of the structure model is accompanied by a rotation of the cross section, which will introduce significant torsional effects on the tunnel joint.

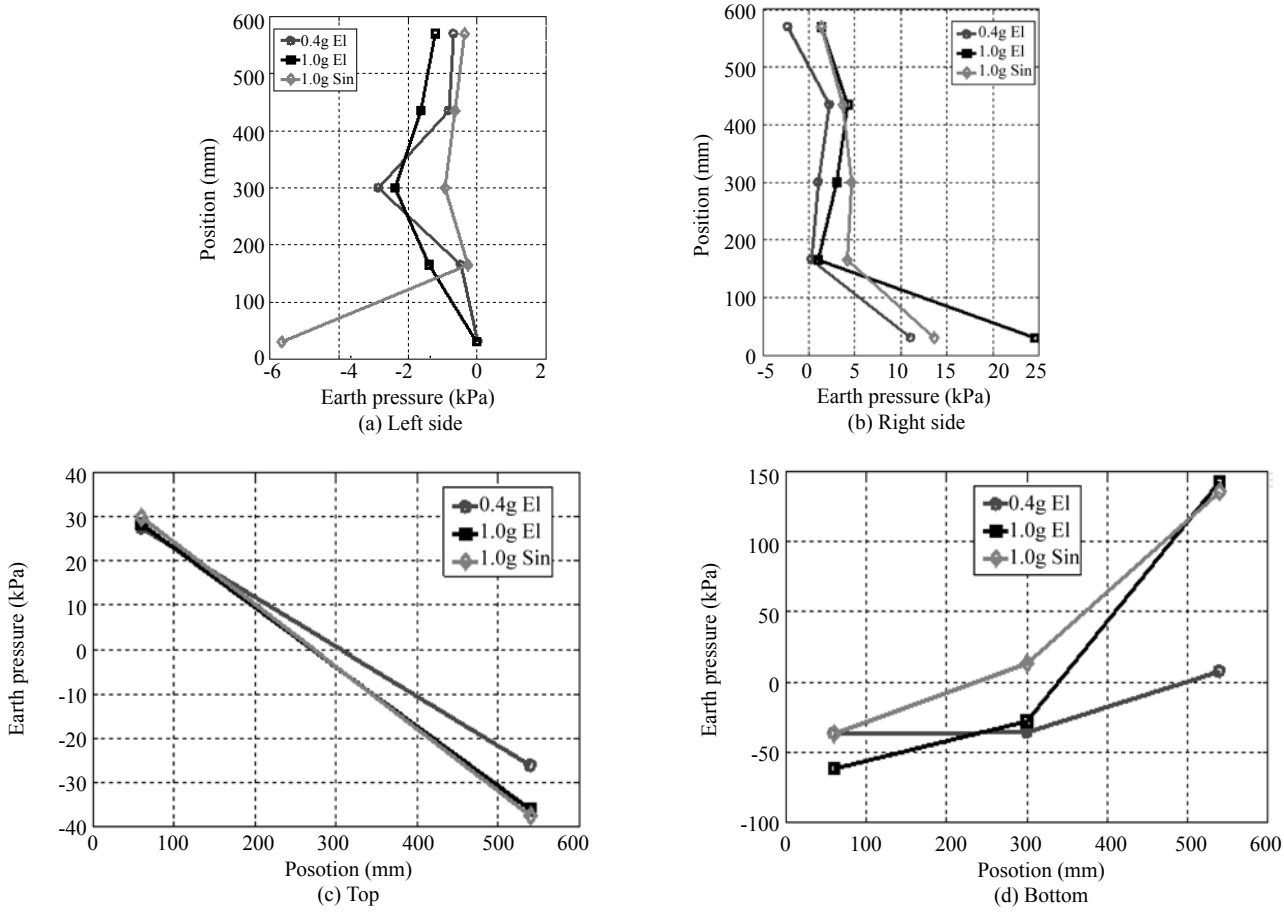

Fig. 8 Maximum soil pressure distribution on soil-structure interface

4 Finite element analysis and comparison with experimental results

4.1 Numerical modeling

A FEM of the tested utility tunnel is established in this section to simulate the shaking table test. Three main factors are considered for the numerical modeling: the laminar shear box, soil-structure interaction and initial stress field. Based on preliminary work in Li *et al*. (2009), a different numerical model is suggested for the shear box. In the new model, a shell element of 1 mm thick is used to simulate the laminar shear box and a unit mass of 126.3 kg is added to the outside of the soil, and the Young's module of the shell element is set to be the same as the soil. Slippage and separation between the soil and the box are ignored. All nodes of the box element at the same height are assumed to have the same displacement along the vibration direction and no displacement in the perpendicular direction. The second is the soil-structure dynamic interaction, which is mainly caused by a nonlinear property of the soil and a contact effect between the soil and the structure. A linear extended Drucker-Prager model is used to consider the

soil constitutive model, and linear and elasticity model to the structure material (see Table 3). Master-slave surfaces are employed to simulate the soil-structure contact effect, with a coefficient of 0.22 between the soil and the structure. The value is determined as 70% of the static friction coefficient (Xu *et al*., 2002). In addition, considering the large influence on coulomb friction force and normal stress on the soil-structure interface, the initial stress is incorporated in initial conditions in the geostatic step, and produces an initial vertical displacement of 0.02668 mm. The soil and the structure are modeled as eight-node 3-D solid elements and four-node shell elements, respectively (see Fig. 9). Finally, the measured acceleration on the shake table in the test is taken as input in the numerical model.

Table 3 Material parameter of soil and structure

	Density (kg/m^3)	Elastic modulus (Mpa)	Poisson's ratio	Inner friction angle (°)	Cohesion (kPa)
Soil	1800	16.5	0.4	27.9	24.4
Structure	2400	30000	0.18	——	——

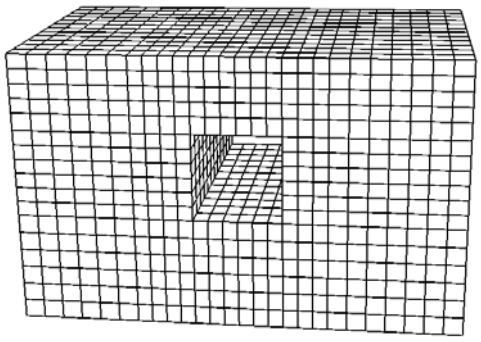

Fig. 9 Meshing of soil-structure-box

4.2 Boundary effect

The boundary effect of the soil container is unavoidable in all soil structure interaction dynamic tests (Prasad *et al*., 2004; Pitilakis *et al*., 2008; Turan *et al*., 2009). The boundary effect includes a direct boundary effect and an indirect boundary effect. The direct boundary effect is caused by end walls perpendicular to the vibration direction while the indirect boundary effect means that the side walls are parallel to the vibration direction. Normally, the direct direction boundary effect is much more significant than the indirect boundary effect. In this paper, an index based on 2-Norms deviation is introduced to quantify the boundary effect of the shear box, and the index μ is calculated using the following equation

$$\mu = \frac{\|X_i - X_0\|}{\|X_0\|} \tag{1}$$

where X_0, X_i are quantities of reference sensor and target sensor, respectively X_0, X_i can be taken as the response time history or even the spectra curve.

Figure 10 shows the 2-norm index μ calculated using acceleration responses, where x_0 is taken as the record of the central sensor, i.e., A2 in the surface layer and A1 in the middle layer. It can be observed that the variation range of μ is 0.04 to 0.28, improved significantly from

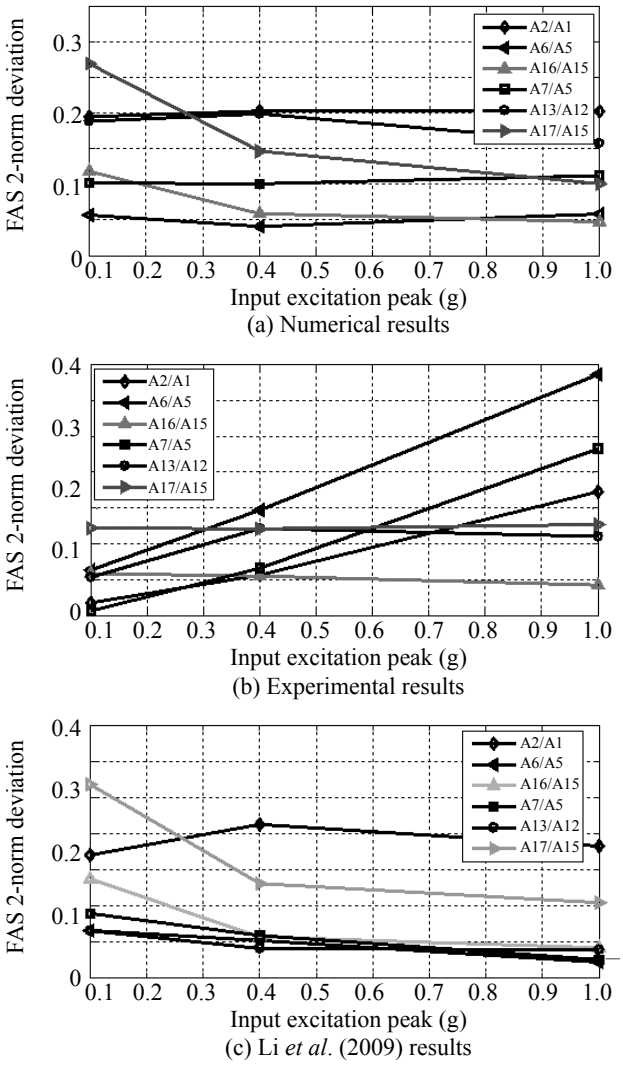

Fig. 10 μ calculated using acceleration responses

Li *et al*. (2009) (see Fig. 10(c)), and the value of μ remains stable under different PGAs, which shows that the boundary effect is small, and numerical results are reasonable.

4.3 Acceleration response

Figure 11 shows a comparison of the amplification factor of acceleration response of the model ground between the numerical and experimental results. Note that the numerical results show good agreement with

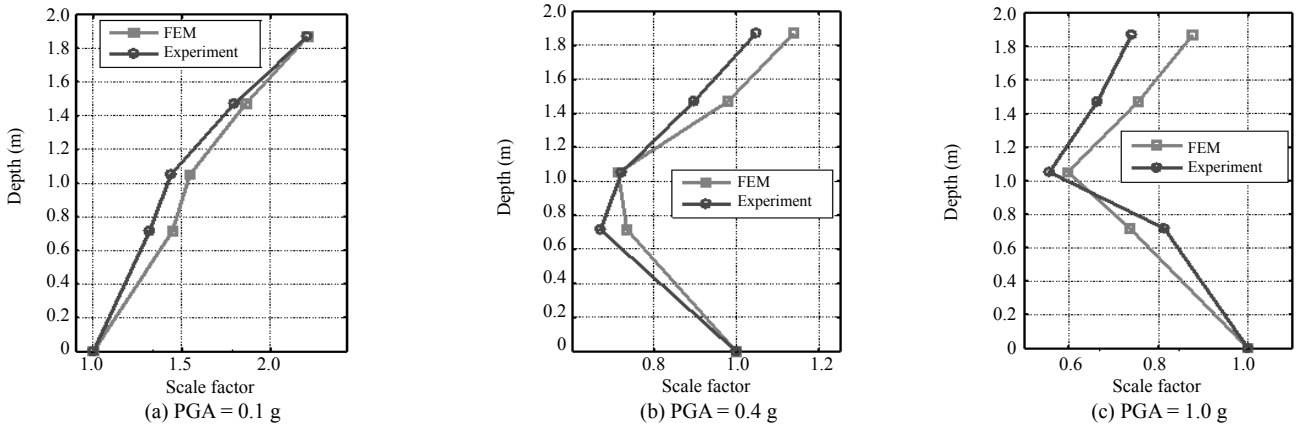

(a) PGA = 0.1 g (b) PGA = 0.4 g (c) PGA = 1.0 g

Fig. 11 Amplification factor of acceleration response of model ground

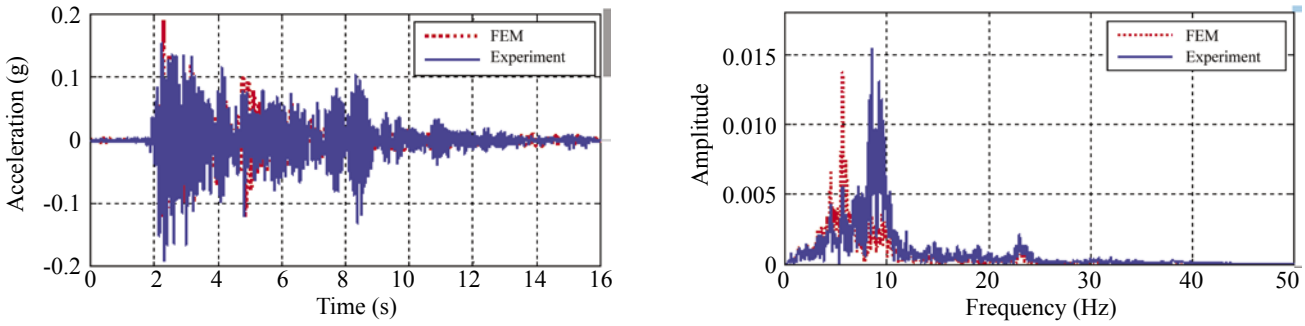

(a) PGA = 0.1 g

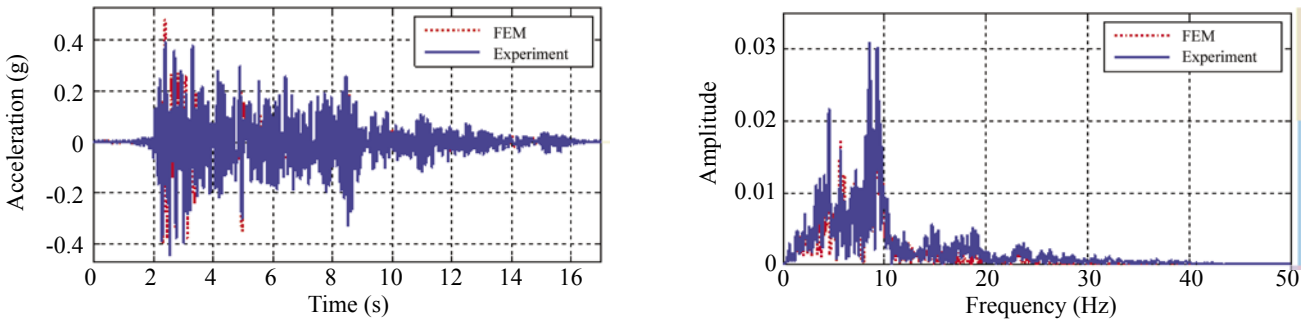

(b) PGA = 0.4 g

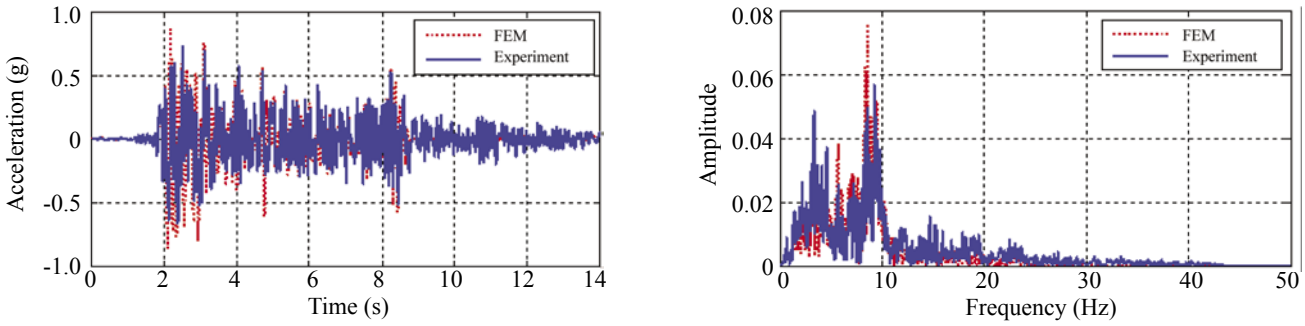

(c) PGA = 1.0 g

Fig. 12 Acceleration time histories measured by sensor A2 and their Fourier spectra

the experimental results. Figure 12 shows a comparison between the time history from sensor A2 and its Fourier spectrum between the numerical and test results. A comparison of maximum acceleration of the model ground and model structure between the numerical and test results is shown in Table 4. It can be seen that the numerical results agree well with the experimental measurements, revealing that the selection of modeling factors is reasonable.

4.4 Displacement response

Figure 13 provides a comparison of the numerical and experimental displacements at the sensor D8 location, which shows that these measurements match quite well. Table 5 provides the calculated maximum displacement of the model ground at the locations of sensors D1 to D8. The results show that for each test case, the difference between the numerical and experimental results is within 1 mm with only one exception.

Table 4 Comparisons of numerical and experimental maximum acceleration responses under different PGAs g

Location of sensors	0.1 g		0.4 g		1.0 g	
	Numerical	Experimental	Numerical	Experimental	Numerical	Experimental
A1	0.18	0.14	0.45	0.40	0.79	0.81
A2	0.19	0.15	0.48	0.39	0.87	0.73
A3	0.20	0.16	0.52	0.41	0.94	0.85
A4	0.20	0.16	0.53	0.40	0.97	0.87
A5	0.16	0.13	0.42	0.36	0.72	0.68
A6	0.16	0.14	0.41	0.33	0.75	0.65
A7	0.17	0.14	0.43	0.35	0.80	0.75
A8	0.17	0.14	0.44	0.35	0.81	0.73
A9	0.12	0.12	0.30	0.28	0.57	0.51
A10	0.12	0.13	0.31	0.30	0.62	0.69
A11	0.12	0.13	0.32	0.30	0.64	0.65
A12	0.10	0.11	0.23	0.26	0.58	0.68
A13	0.10	0.11	0.25	0.30	0.57	0.72
A14	0.10	0.11	0.26	0.29	0.57	0.68
A15	0.07	0.09	0.25	0.31	0.65	0.68
A16	0.08	0.09	0.25	0.31	0.67	0.68
A17	0.08	0.09	0.24	0.31	0.65	0.75
A18	0.08	0.09	0.24	0.32	0.62	0.79
A24	0.16	0.09	0.42	0.23	0.72	0.38
MA1	0.16	0.13	0.42	0.34	0.73	0.63
MA2	0.07	0.07	0.28	0.28	0.73	0.73
MA3	0.07	0.07	0.28	0.28	0.73	0.74

Table 5 Comparisons of numerical and experimental maximum displacement responses under different PGAs mm

Location of sensors	0.1 g		0.4 g		1.0 g	
	Numerical	Experimental	Numerical	Experimental	Numerical	Experimental
D1	2.19	1.73	9.05	8.79	18.78	21.81
D2	2.46	1.88	9.24	8.73	18.61	21.50
D3	2.61	1.76	9.31	8.40	18.59	19.89
D4	2.73	1.73	9.40	7.94	18.60	18.42
D5	2.86	1.82	9.47	7.55	18.62	19.01
D6	2.96	1.69	9.57	7.37	18.76	18.12
D7	3.08	1.81	9.74	7.44	19.14	18.30
D8	3.15	1.75	9.89	7.63	19.41	18.50

4.5 Structural strain

Figure 14 is the time history of concrete strain at the location of sensor CS4, which shows that the numerical and experimental results match well, and the difference between the two increases with the PGA. Table 6 further shows the measured and computed maximum strain at locations of CS1 – CS7. Note that the calculated strain also matches quite well with the measured values at all sensors locations.

Figure 15 shows the maximum strain distribution of the outer slab at the time of maximum vertical displacement of structure, which shows that the strain is larger at the corner and smaller at the mid-height of the side slab, while the strain of the top slab is concentrated in the middle. This result is also in accordance with the test observation.

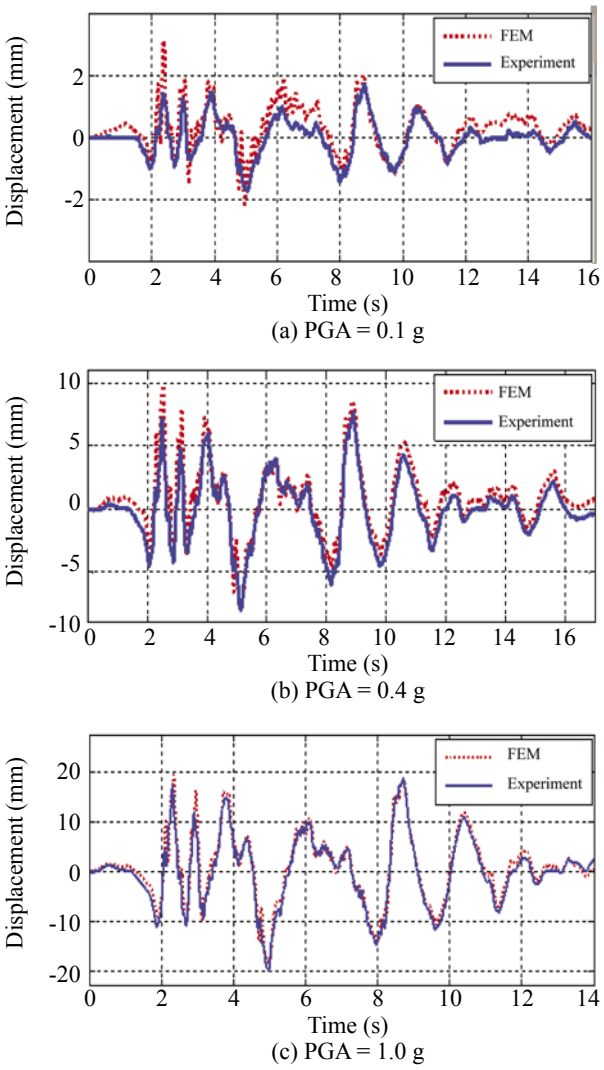

Fig. 13 Displacement time histories at location of sensor D8

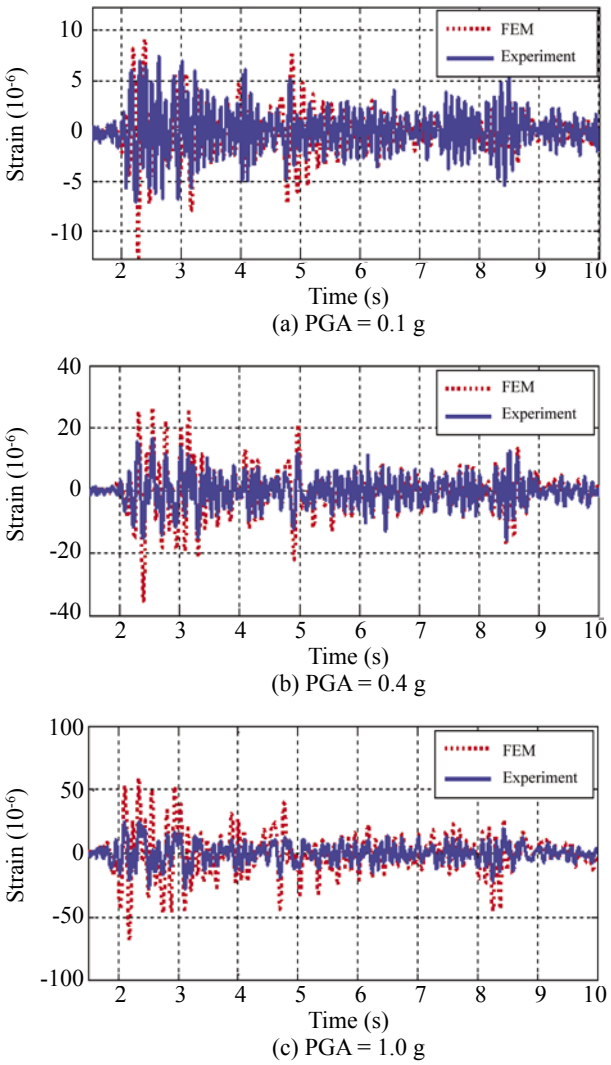

Fig. 14 Time histories of concrete strains at location of sensor CS4

Table 6 Comparisons of numerical and experimental maximum strain responses under different PGAs 10^{-6}

Location of sensors	0.1 g		0.4 g		1.0 g	
	Numerical	Experimental	Numerical	Experimental	Numerical	Experimental
CS1	15.39	11.71	43.30	14.35	76.70	22.47
CS3	11.39	12.30	32.96	16.16	69.08	27.41
CS4	9.22	11.69	26.76	15.75	59.39	27.28
CS6	12.44	6.09	34.56	10.72	64.57	17.21
CS7	9.85	6.45	27.48	12.36	47.78	20.06
CS9	7.08	6.10	19.93	10.08	43.02	17.36

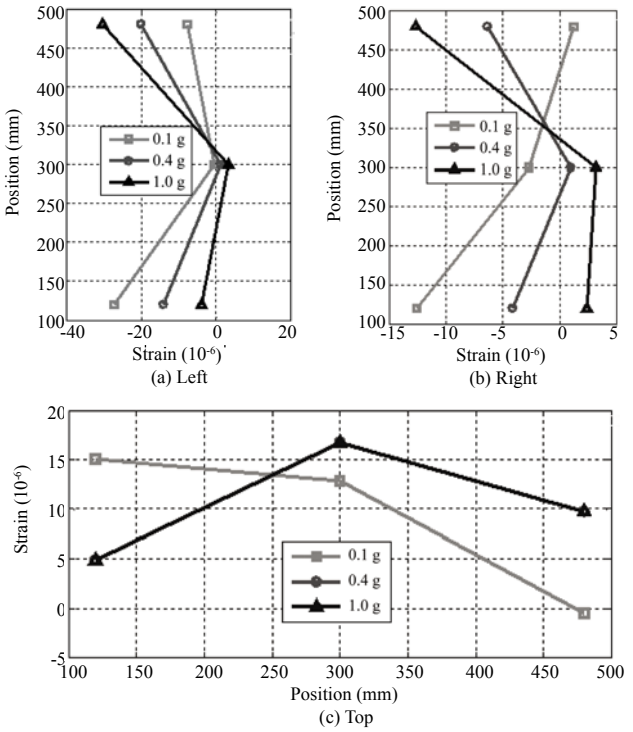

Fig. 15 Strain distribution along different sides of the model structure at the time of maximum interlaminar displacement occuring

4.6 Earth pressure on the soil-structure interface

Contact pressure, which is defined by the normal contact force divided by the element area at the contact node, was calculated in the FEM analysis, and compared with the soil pressure measured in the test, i.e., from all the EP sensors (see Fig. 16). The comparison shows a good agreement between the two under low input excitation levels. It is assumed that the dynamic earth pressure triggered by a seismic wave has an important effect on the underground utility tunnels. Further research on the effect of dynamic earth pressure on undrground structures is necessary.

5 Conclusions

A study of the seismic response of an underground utility tunnel using shaking table testing and numerical analysis is described in this paper. From the shaking table testing, it was observed that: (1) the acceleration response of a structure is slightly lower than the surrounding soil; (2) the maximum internal force of an underground utility tunnel appears at its corner, and the internal force increases with the input PGA; (3) with the increase of PGA, the earth pressure on the soil-structure interface increases, however, the distribution pattern of the earth pressure on a side slab is different from on the top or bottom slab; and (4) the displacement drift between the top and bottom slab is produced under horizontal earthquake excitation, accompanied by

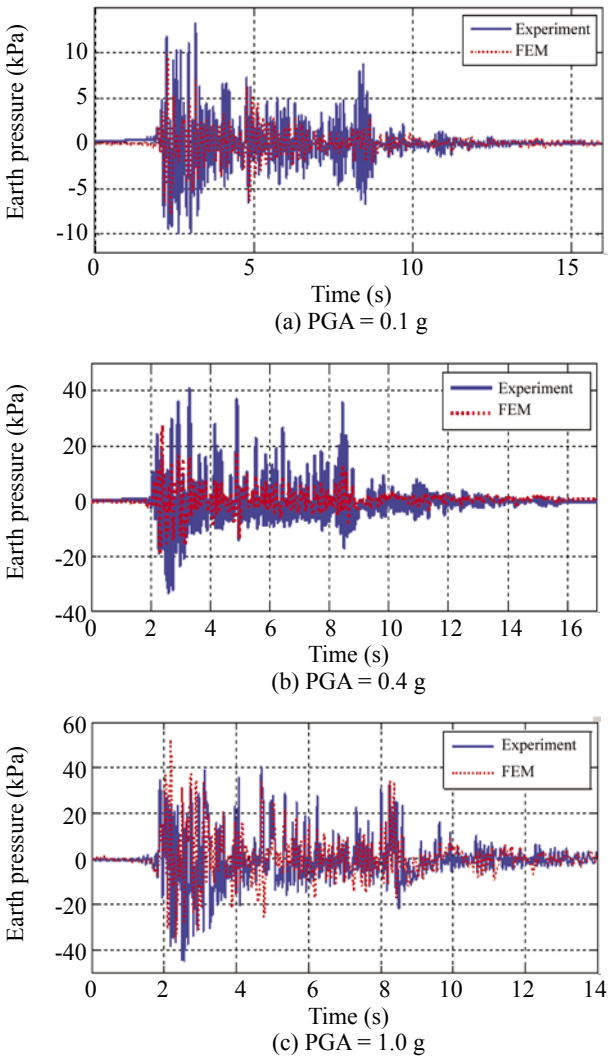

Fig. 16 Earth pressure time histories at location of sensor EP35

rotation of the cross section.

A numerical model based on the shaking table test of an underground utility tunnel is established. The boundary effect was evaluated by the 2-norm index. The results demonstrated that the modeling of the laminar shear box does not impose significant boundary effects on the model ground. The numerical results were compared with experiment measurements in terms of displacement, acceleration and amplification factor, strain, and earth pressure on the surface between the soil and the structure. The comparisons show the numerical results are in good agreement with the test results, which serves as a good verification of the test and a sound foundation for further investigations. Numerical results showed that the dynamic earth pressure triggered by a seismic wave is the main factor in underground utility tunnel damage.

As a new type of long line structure, further studies are being conducted on the seismic responses of an underground utility tunnel under non-uniform earthquake excitation.

Acknowledgement

The authors gratefully acknowledge the financial support from the Key Project in the National Science & Technology Pillar Program (Grant NO. 2006BAJ03B03) and Research Fund for Young Teachers supported by the State Key Laboratory for Disaster Reduction in Civil Engineering (SLDRCE08-C-03).

References

Chen Jun, Shi Xiaojun and Li Jie (2010), "Shaking Table Test of Utility Tunnel under Non-uniform Earthquake Wave Excitation," *Soil Dynamics and Earthquake Engineering*, **30**(11): 1400–1416.

Hashash Y, Hook J, Schmidt B and Yao J (2001), "Seismic Design and Analysis of Underground Structures," *Tunnelling and Underground Space Technology*, **16**(4): 247–293.

JSCE (1999), "Investigation Report on Hyogoken-nambu Earthquake – Analysis of Civil Structure Damage, Chapter 5: Tunnel and Underground Structure," *Japan Society of Civil Engineer.* (in Japanese)

Li Jie, Yue Qingxia and Chen Jun (2009), "Research on Shaking-table Test and Finite Element Numerical Simulation of Utility Tunnel," *Journal of Earthquake Engineering and Engineering Vibration*, **29**(4): 41–45. (in Chinese)

Nakanura G, Kawashima K *et al*. (2006), "Evaluation on Seismic Retrofit Measures for Common Utility Tunnels Based on Cyclic Loading Tests," *Proceeding of Civil Engineering Institute*, **62**(3): 489–508. (in Japanese)

Nishioka T and Unjo S (2002), "Simplified Evaluation Method for the Seismic Performance of Common Utility Boxes with Rectangular Cross Section," *Journal of Structure Engineering*, **48**(A): 1461–1468. (in Japanese)

Pitilakis D, Dietz M, Wood DM *et al*. (2008), "Numerical Simulation of Dynamic Soil-structure Interaction in Shaking Table Testing," *Soil Dynamics and Earthquake Engineering*, **28**(6): 453–467.

Prasad SK, Towhata I, Chandradhara GP and Nanjundaswamy P (2004), "Shaking Table Tests in Earthquake Geotechnical Engineering," *Current Science*, **87**(10): 1398–1404.

PWRI (2001), "Damage Analysis and Seismic Performance Assessment of Utility Tunnel in Hogoken-Nambu Earthquake," *Report No. 3821*, Public Works Research Institute, Japan. (in Japanese)

Schiff AJ (1998), "Hyogoken-Nanbu (Kobe) Earthquake of January 17, 1995 Lifeline Performance," *Technical Council on Lifeline Earthquake Engineering Monograph*, No. 14, published by ASCE, September.

Shi Xiaojun, Chen Jun and Li Jie (2008), "Shaking Table Test of Underground Utility Tunnel," *Earthquake Engineering and Engineering Vibration*, **28**(6): 116–123. (in Chinese)

Turan A, Hinchberger SD and Naggar HE (2009), "Design and Commissioning of a Laminar Soil Container for Use on Small Shaking Tables," *Soil Dynamics and Earthquake Engineering*, **29**(2): 404–414.

Xu Hongfa, Hu Huajie, Guo Shaoping and Liao Tieping (2002), "Study on the Parameters of Pile Soil Contact Surface Element," *Exploration Engineering*, **29**(5): 10–12. (in Chinese)

Yue Qingxia and Li Jie (2009), "Research on Utility Tunnel Seismic Response," *Journal of Tongji University* (*Natural Science*), **37**(3): 285–290. (in Chinese)